Supplementary Material

Ferrocene-loaded Glycerogel Dressing for Reactive Oxygen Species-modulated Active Wound Healing

Jiwon, Kang[a,b,‡], Sohyun Yu[a,c,‡], Jisu Kim[a,c,‡], Seongwoo Yang[d,e,‡], Won Il Choi[a], Jinhan Cho[b], Jeonghun Kim[e,*], Daekyung Sung[a,*], Byoung Soo Kim[a,*]

[a] Center for Bio-Healthcare Materials, Bio-Convergence Materials R&D Division, Korea Institute of Ceramic Engineering and Technology, Chungbuk, 28160, Republic of Korea

[b] School of Chemical and Biomolecular Engineering, Korea University, 145, Anam-ro, Seongbuk-gu, Seoul 02841, Republic of Korea

[c] School of Chemical and Biomolecular Engineering, Yonsei University, 50 Yonsei-ro, Seodaemun-gu, Seoul 03722, Republic of Korea

[d] Department of Medical Device Management and Research, SAIHST, Sungkyunkwan University, Seoul 06355, Republic of Korea

[e] Biomedical Engineering Research Center, Samsung Medical Center, Seoul 06351, Republic of Korea

‡These authors contributed equally.

***Corresponding Authors**

Byoung Soo Kim

Center for Bio-Healthcare Materials, Bio-Convergence Materials R&D Division, Korea Institute of Ceramic Engineering and Technology, Chungbuk, 28160, Republic of Korea

bskim@kicet.re.kr

Table S1. Monomer feeds and resultant copolymer compositions, along with number-average molecular weight (Mn) and dispersity ($Đ_M$ = Mw/Mn) for copolymers synthesized at different ferrocene contents (mol%). Feed ratios are given as MA:FMMA for FP and MA:PEGMA:FMMA for FP-PEG.

Sample	Monomer feed composition (mol%)			Copolymer composition (mol%)			Conversion (%)	Mw (g/mol)	$Đ_M$
	MAA	PEGMA	FMMA	MAA	PEGMA	FMMA			
FP	83.33	0	16.67	84.11	0	15.89	99.86	5,150	1.60
FP-PEG	41.67	41.67	16.67	42.02	41.3	16.68	99.78	12,803	1.72

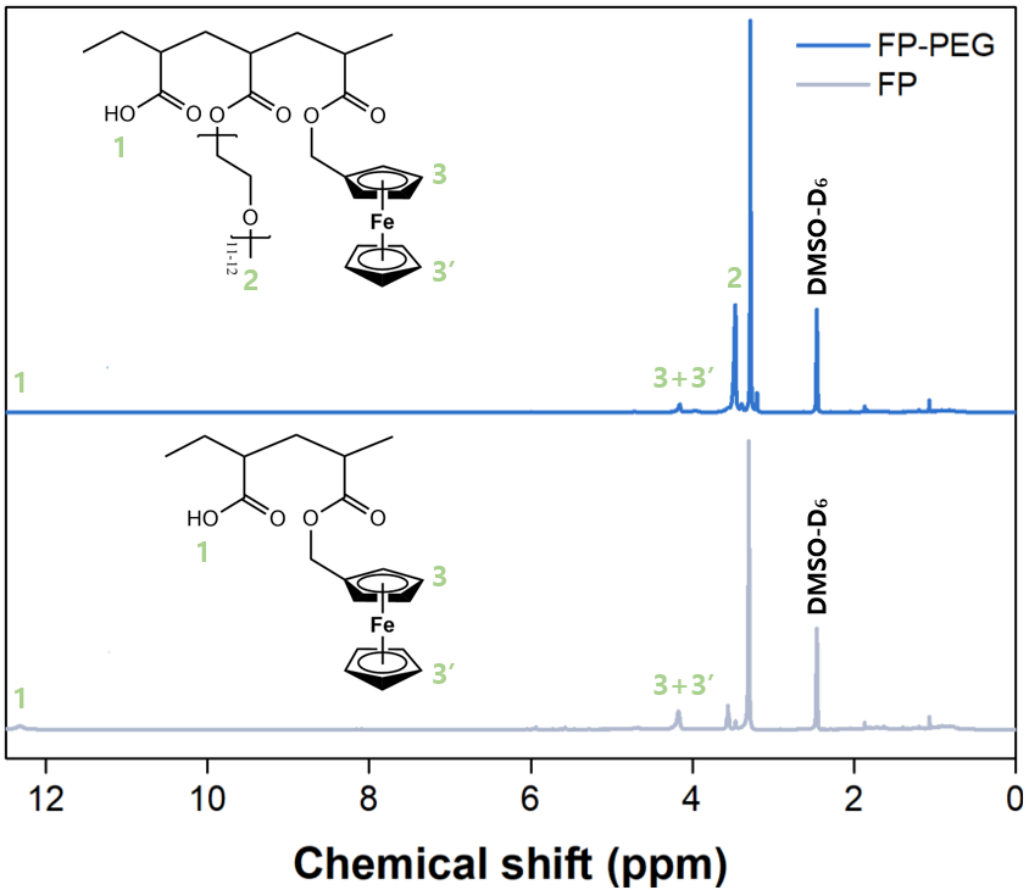

Figure S1. ^{1}H NMR spectra of ferrocene-based polymer (FP) and FP-PEG confirming successful copolymerization of ferrocenylmethyl methacrylate (FMMA), methacrylate (MA), and poly(ethylene glycol) methacrylate (PEGMA) units. Characteristic signals corresponding to each segment are highlighted.

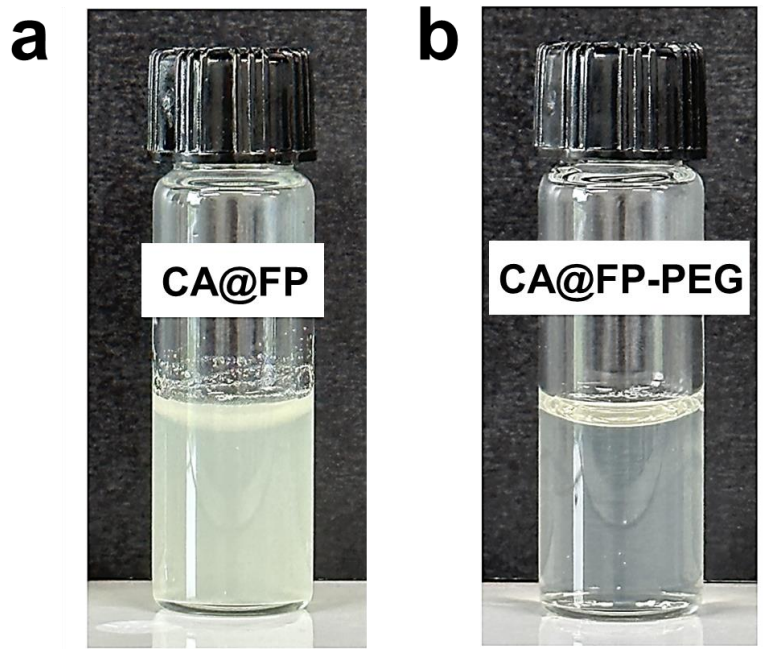

Figure S2. Optical appearance of nanoparticle dispersions after *Centella asiatica* (CA) loading. Photographs of (a) ferrocene-based polymer (FP) and (b) FP-PEG nanoparticle suspensions with CA. CA@FP suspensions appear turbid, whereas CA@FP-PEG suspensions remain optically clear, indicating more efficient encapsulation and improved dispersion stability.

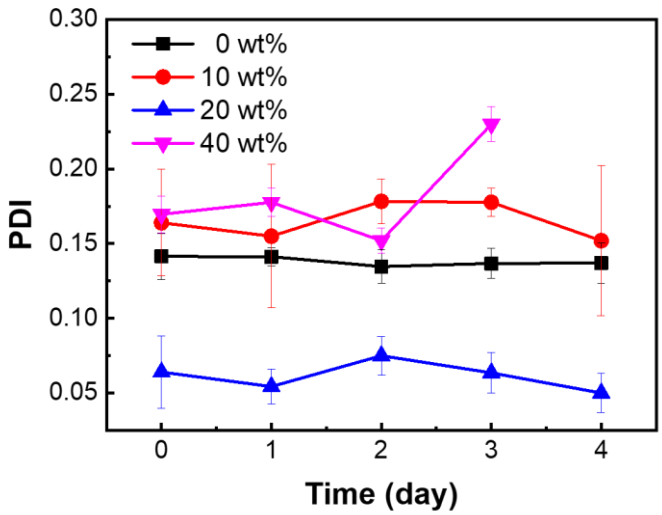

Figure S3. Dynamic light scattering (DLS)-derived, intensity-weighted hydrodynamic size distributions of CA@FP-PEG nanoparticles at *Centella asiatica* (CA) loadings of 0, 10, 20, and 40 wt% relative to polymer.

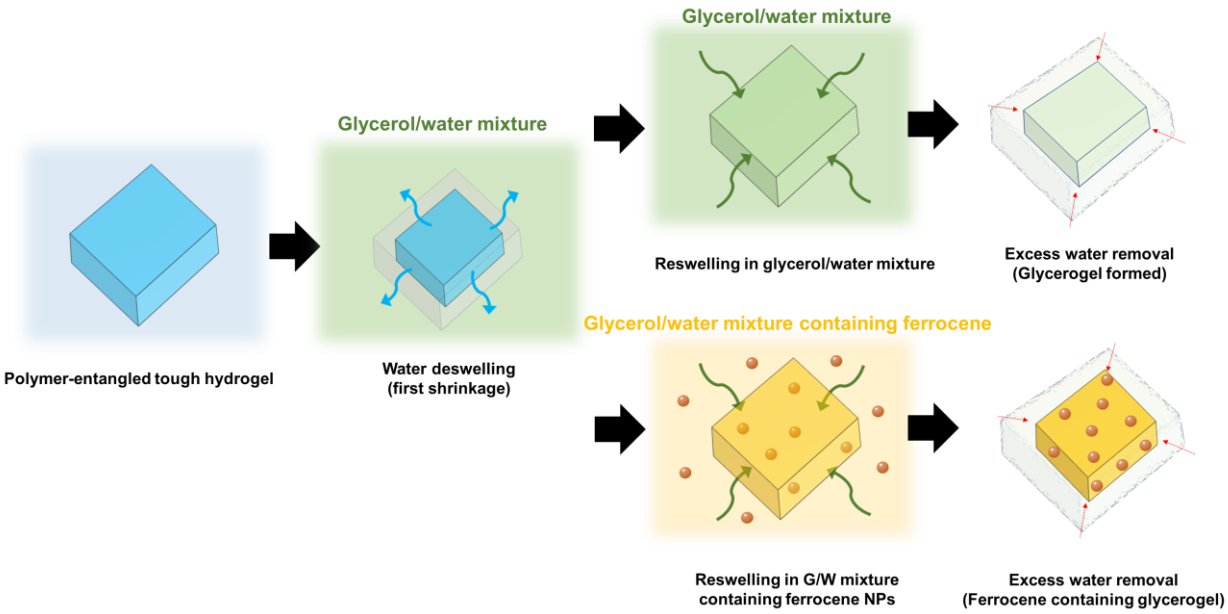

Figure S4. Preparation of adhesive glycerogel and integration of CA@FP-PEG nanoparticles.

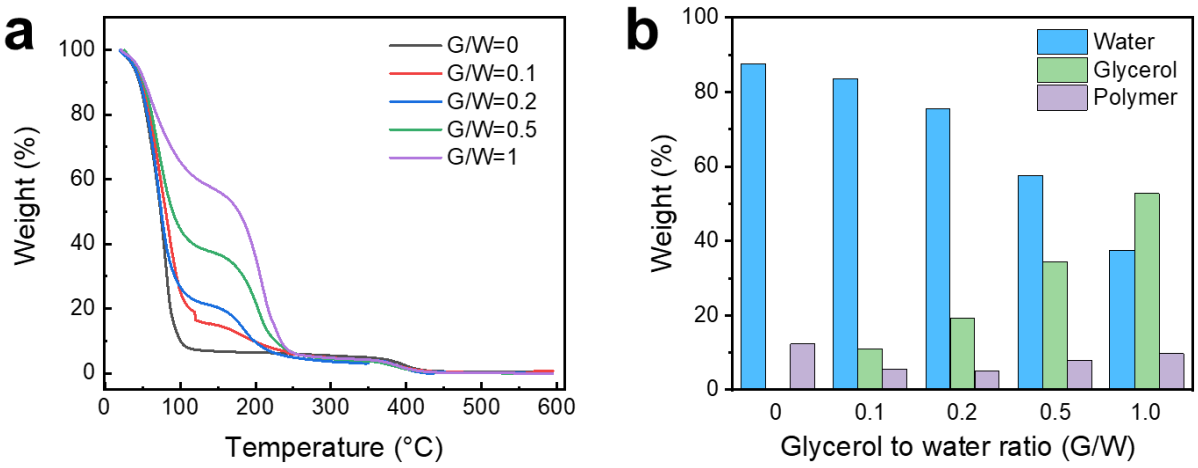

Figure S5. (a) Thermogravimetric analysis (TGA) traces used to estimate residual water and glycerol contents after equilibration at the indicated G/W ratios. (b) Quantified fractions of water and glycerol obtained from TGA analysis.

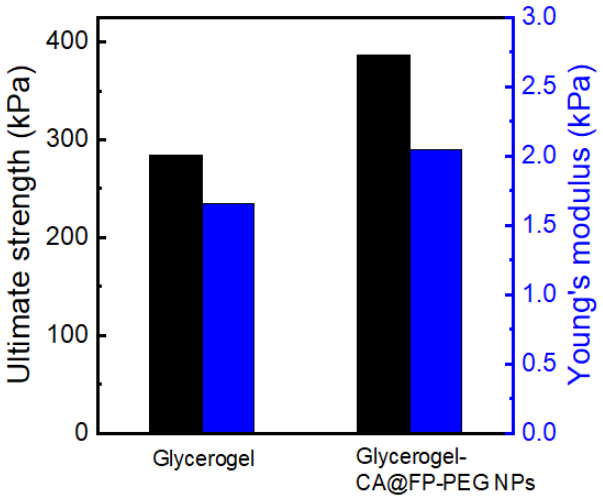

Figure S6. Mechanical characterization of glycerogel and glycerogel-CA@FP-PEG NPs (G/W = 0.2): summary of ultimate tensile strength and Young's modulus.

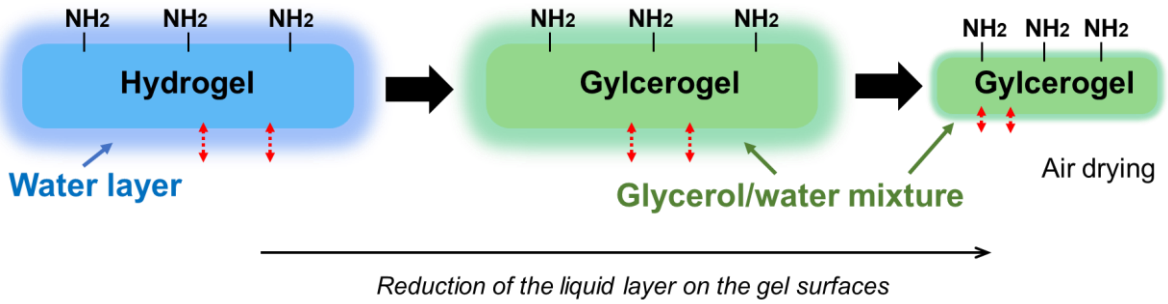

Figure S7. Possible mechanism of adhesion enhancement in glycerogel. Partial dehydration during excess-water removal locally concentrates surface functional groups (amide) near the interface. Schematic cross-sections before and after excess-water removal illustrate thinning of the interfacial water-bound layer and closer gel–substrate contact.

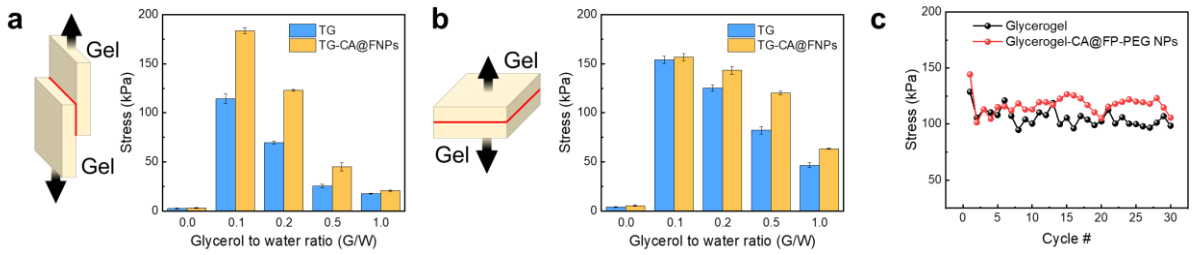

Figure S8. (a) Lap-shear and (b) tensile adhesion strengths between gels. (c) Cyclic adhesion performances of glycerogel and glycerogel-CA@FP-PEG NPs (G/W = 0.2) over 30 attach–detach cycles.